On the Choice of Norm in Finite Control Set Model Predictive Control

Petros Karamanakos, *Member, IEEE*, Tobias Geyer, *Senior Member, IEEE*,
and Ralph Kennel, *Senior Member, IEEE*

Abstract—In power electronics, the ℓ_1-norm (instead of the squared ℓ_2-norm) is often used in the objective function of model predictive controllers (MPCs) with reference tracking. Although the ℓ_1-norm is preferred for its computational simplicity, it might lead to a performance deterioration and closed-loop instability. This paper analyzes the root cause for this and discusses the benefits of using the ℓ_2-norm instead. Given the theoretical nature of this paper, a power electronics-oriented case study is employed to visualize and exemplify—through examples and simulations—the mathematical concepts and arguments presented. To this end, a variable speed drive system with a three-level voltage source inverter serves as an illustrative example to clearly demonstrate the effectiveness of using the ℓ_2-norm.

Index Terms—Model predictive control (MPC), optimal control, objective function, system stability

I. Introduction

MODEL predictive control (MPC) [1], [2] is a well-established advanced control methodology that was developed in the process control industry in the 1970s. Over the years, it paved its way into many disciplines thanks to its numerous advantages. MPC is suitable for nonlinear multiple-input multiple-output (MIMO) plants with complex dynamics. Furthermore, constraints can be explicitly or implicitly imposed and met, allowing the plant to be operated at its physical and safety limits. As a result, favorable operation can be obtained without the need to oversize system components while meeting operational limits.

An objective function is formulated that captures the control objectives and the plant behavior is described by (discrete-time) dynamical equations. Additional hard or soft constraints on the state variables and the manipulated variables (the control inputs) can be added. By solving the resulting constrained optimization problem in real time at each time step, a sequence of control actions over a finite prediction horizon is obtained, which are optimal with respect to the objective function. In accordance with the receding horizon policy, only the first element of the optimal sequence of control actions is applied to the plant. At the next step, the optimization procedure is repeated with new measurements or estimates over a horizon that is shifted by one step [3], [4]. The receding horizon policy

P. Karamanakos is with the Faculty of Computing and Electrical Engineering, Tampere University of Technology, Tampere 33101, Finland; e-mail: p.karamanakos@ieee.org

T. Geyer is with ABB Corporate Research, Baden-Dättwil 5405, Switzerland; e-mail: t.geyer@ieee.org

R. Kennel is with the Chair of Electrical Drive Systems and Power Electronics, Technische Universität München, Munich 80333, Germany; e-mail: ralph.kennel@tum.de

adds feedback and makes MPC robust to model mismatches, uncertainties and disturbances.

The conceptual simplicity of MPC and its aforementioned advantages attracted the interest of the power electronics community in the early 2000s, see [5], [6] and the survey papers [7]–[9]. In the last decade, MPC has been extensively discussed for a variety of power electronic applications and control tasks. Prominent examples include, among others, current control of inverters [10]–[12], power control of grid-connected converters [13], [14], voltage control of dc-dc converters [15], [16], and torque [17]–[19], current [20], and flux [21] control of electrical drives. In most of these references, *direct* MPC with reference tracking is used—the so-called finite control set MPC (FCS-MPC). This implies that the switches of the converter are directly manipulated, avoiding an explicit modulation stage. This simplifies the design stage.

However, since the control actions have to be computed in power electronic systems in a matter of some tens of microseconds, control designers often resort to far-reaching simplifications, which often cause—knowingly or unknowingly—significant performance degradations. Among the most frequent simplifications is the use of overly short prediction horizons to limit the computational complexity. The pitfall of this approach is a degradation of the steady-state performance (current distortions per switching frequency), as shown e.g., in [22], [23]. Moreover, the penalty on the switching effort is often omitted in FCS-MPC formulations, which is in violation of the optimal control paradigm [2]. As a result, the switching frequency is merely indirectly controlled through the chosen sampling interval, and the ratio between current distortions and switching frequency is suboptimal.

Another widely used simplification is the use of the ℓ_1-norm in the objective function, i.e., the sum of the *absolute values* of the predicted tracking error components, see [8] and references therein. The ℓ_1-norm is considered to require fewer computations than the squared ℓ_2-norm, which is the sum of *squares* of the tracking error components. Apart from a preliminary discussion in [24, Chap. 10], it is commonly believed in the power electronics community that the choice of norm is merely a subtlety that does not influence the controller performance. This belief is wrong, as will be shown in this paper for linear systems with integer inputs and a one-step predictive current controller. Indeed, when using a nonzero penalty on the switching effort, the ℓ_1-norm can lead to closed-loop instability, severely affecting the steady-state performance. A critical value $\lambda_{u,\mathrm{crt}}^{(1)}$ will be derived for the ℓ_1-norm; if the penalty on switching exceeds this value, then

the controller is unable to switch altogether, always leading to instability. In contrast to this, the ℓ_2-norm will always ensure practical stability [25], regardless of the penalty on switching. This paper describes the underlying root cause and shows the impact the selection of the norm has on the closed-loop stability. To this end, a medium-voltage (MV) variable speed drive system is used as an illustrative example. We would like to emphasize that the results in this paper are valid for all linear systems with integer inputs.

This paper is structured as follows. The systems under consideration, the formulation of the MPC problem based on the ℓ_1- and ℓ_2-norm, respectively, and the consequent impact of the choice of norm are analyzed in Section II. The drive system case study is outlined in Section III, whereas the optimization problem underlying predictive current control with reference tracking is introduced in Section IV. A discussion on the impact of norms on the chosen case study follows in Section V. In Section VI, the performance of the MPC strategy is demonstrated for both norms and the benefits of using the ℓ_2-norm are highlighted. Conclusions are drawn in Section VII.

II. Impact of the Choice of Norm: Analysis

This section analyzes the impact of the choice of norm on the closed-loop performance of the system controlled by FCS-MPC. Without loss of generality, a three-phase power electronic system is considered. Furthermore, the modeling and analysis are done in the $\alpha\beta$-plane[1]. Finally, all quantities are assumed to be normalized, i.e., all derivations and results are in the per unit (p.u.) system.

A. Background and Prerequisites

The system under consideration is described by the following continuous-time linear dynamical system

$$\frac{d\boldsymbol{x}(t)}{dt} = \boldsymbol{F}\boldsymbol{x}(t) + \boldsymbol{G}'\boldsymbol{u}(t) \tag{1a}$$

$$\boldsymbol{y}(t) = \boldsymbol{C}\boldsymbol{x}(t). \tag{1b}$$

In (1) $\boldsymbol{x} \in \mathbb{R}^{n_x}$ is the n_x-dimensional state, and $\boldsymbol{u} = [u_a \ u_b \ u_c]^T \in \mathcal{U} = \mathcal{U} \times \mathcal{U} \times \mathcal{U} = \mathcal{U}^3$, with $\mathcal{U} \subset \mathbb{Z}$, is the integer-valued input vector that can be interpreted as the three-phase switch position. The n_y system outputs are aggregated to the output vector $\boldsymbol{y} \in \mathbb{R}^{n_y}$; the outputs are considered to be a subset of the state variables, i.e., monomials in the state variables. Finally, the system matrix $\boldsymbol{F} \in \mathbb{R}^{n_x \times n_x}$, the input matrix $\boldsymbol{G}' = \boldsymbol{GK}$, with $\boldsymbol{G} \in \mathbb{R}^{n_x \times 2}$, and the output matrix $\boldsymbol{C} \in \mathbb{R}^{n_y \times n_x}$ can be either time-invariant or time-varying without affecting the analysis presented hereafter. For

[1]To simplify the modeling and the controller design, all variables $\boldsymbol{\xi}_{abc} = [\xi_a \ \xi_b \ \xi_c]^T$ in the three-phase (abc) system are transformed to $\boldsymbol{\xi}_{\alpha\beta} = [\xi_\alpha \ \xi_\beta]^T$ in the stationary orthogonal $\alpha\beta$ system, i.e., $\boldsymbol{\xi}_{\alpha\beta} = \boldsymbol{K}\boldsymbol{\xi}_{abc}$, with $\boldsymbol{K}$ being the transformation matrix

$$\boldsymbol{K} = \frac{2}{3} \begin{bmatrix} 1 & -\frac{1}{2} & -\frac{1}{2} \\ 0 & \frac{\sqrt{3}}{2} & -\frac{\sqrt{3}}{2} \end{bmatrix}.$$

Note that throughout the text, vectors in the $\alpha\beta$-plane are denoted with the corresponding subscript, whereas for vectors in the abc-plane the subscript is omitted.

matrix $\boldsymbol{G}$, it is assumed that its columns $\boldsymbol{g}_i$, $i = 1, 2$, are orthogonal, i.e., $\boldsymbol{g}_1^T \boldsymbol{g}_2 = 0$.

MPC requires the prediction model of the system to be in the discrete-time domain. Hence, (1) is discretized with the exact Euler discretization. This leads to the state-space representation

$$\boldsymbol{x}(k+1) = \boldsymbol{A}\boldsymbol{x}(k) + \boldsymbol{B}'\boldsymbol{u}(k), \tag{2a}$$

$$\boldsymbol{y}(k) = \boldsymbol{C}\boldsymbol{x}(k), \tag{2b}$$

with $\boldsymbol{A} = e^{\boldsymbol{F}T_s}$, $\boldsymbol{B}' = \boldsymbol{BK}$ and $\boldsymbol{B} = -\boldsymbol{F}^{-1}(\boldsymbol{I} - \boldsymbol{A})\boldsymbol{G}$. $\boldsymbol{I}$ is the identity matrix of dimension $n_x \times n_x$, e is the matrix exponential, T_s is the sampling interval, and $k \in \mathbb{N}$ denotes the discrete time step.

For direct MPC (FCS-MPC) with output reference tracking and a penalty on the control effort, which is imposed by penalizing the difference between two consecutive three-phase switch positions $\Delta\boldsymbol{u}(k) = \boldsymbol{u}(k) - \boldsymbol{u}(k-1)$, the objective function $J_p : \mathbb{R}^{n_y} \times \mathcal{U} \to \mathbb{R}^+$ results

$$J_p(k) = || \underbrace{\boldsymbol{y}_{\text{ref}}(k+1) - \boldsymbol{y}(k+1)}_{\boldsymbol{y}_{\text{err}}(k+1)} ||_p^p + \lambda_u ||\Delta\boldsymbol{u}(k)||_p^p. \tag{3}$$

Function (3) can be based either on the ℓ_1- or the (squared) ℓ_2-norm by setting $p = 1$ or $p = 2$, respectively[2]. The weighting factor $\lambda_u \in \mathbb{R}^+$ is a tuning parameter, which determines the trade-off between the tracking accuracy (i.e., the deviation of the output variables from their references) and the switching effort (i.e., the switching frequency), whereas—for sake of simplicity—the output errors are equally prioritized[3].

To compute the optimal control input $\boldsymbol{u}^*(k)$ which minimizes (3), the following integer optimization problem is solved in real time

$$\underset{\boldsymbol{u}(k) \in \mathcal{U}}{\text{minimize}} \quad J_p(k) \tag{4a}$$

$$\text{subject to} \quad \boldsymbol{x}(k+1) = \boldsymbol{A}\boldsymbol{x}(k) + \boldsymbol{B}'\boldsymbol{u}(k) \tag{4b}$$

$$\boldsymbol{y}(k) = \boldsymbol{C}\boldsymbol{x}(k) \tag{4c}$$

$$||\Delta\boldsymbol{u}(k)||_\infty \le 1. \tag{4d}$$

The optimal solution $\boldsymbol{u}^*(k)$ is typically found by enumerating all admissible (i.e., *feasible*) switch positions, i.e., the switch positions $\boldsymbol{u}(k) \in \mathcal{U}_{\text{adm}}(k)$, with $\mathcal{U}_{\text{adm}}(k) = \{\boldsymbol{u}(k) \mid \boldsymbol{u}(k) \in \mathcal{U}, ||\Delta\boldsymbol{u}(k)||_\infty \le 1\}$ being the set of three-phase admissible switch positions, defined as the Cartesian product of the admissible *phase* switch positions $\mathcal{U}_{\text{adm},x}$, $x \in \{a, b, c\}$, i.e., $\mathcal{U}_{\text{adm}}(k) = \mathcal{U}_{\text{adm},a}(k) \times \mathcal{U}_{\text{adm},b}(k) \times \mathcal{U}_{\text{adm},c}(k)$. Finally, it should be pointed out that the constraint (4d) is added to limit the switching transition per phase

[2]Note that in (3) the prediction horizon is set equal to one time step ($N = 1$) to simplify the analysis that follows. However, the extension to longer prediction horizons is straightforward.

[3]If prioritization among the different output errors was required then the first term in (3) would become $||\boldsymbol{\Lambda}\boldsymbol{y}_{\text{err}}(k+1)||_p^p$ by introducing the diagonal weighting matrix $\boldsymbol{\Lambda} = \text{diag}(\lambda_1, \lambda_2, \ldots, \lambda_{n_y})$, with $\lambda_i \in \mathbb{R}^+$, $i = 1, \ldots, n_y$. Notwithstanding the foregoing, the core of the analysis that follows remains intact and the conclusions drawn still hold true.

to one step and to thus avoid a shoot through[4].

B. Analysis

As a preparatory step, we write the output term in (3) as

$$
\begin{aligned}
\boldsymbol{y}(k+1) &= \boldsymbol{C}\boldsymbol{A}\boldsymbol{x}(k) + \boldsymbol{C}\boldsymbol{B}'\boldsymbol{u}(k) \\
&= \boldsymbol{C}\boldsymbol{A}\boldsymbol{x}(k) + \boldsymbol{C}\boldsymbol{B}'\boldsymbol{u}(k-1) + \boldsymbol{C}\boldsymbol{B}'\Delta\boldsymbol{u}(k),
\end{aligned} \tag{5}
$$

and the objective function becomes

$$
\begin{aligned}
J_p(k) = \|\boldsymbol{y}_{\text{ref}}(k+1) &- \boldsymbol{C}\boldsymbol{A}\boldsymbol{x}(k) - \boldsymbol{C}\boldsymbol{B}'\boldsymbol{u}(k-1) \\
&- \boldsymbol{C}\boldsymbol{B}'\Delta\boldsymbol{u}(k)\|_p^p + \lambda_u\|\Delta\boldsymbol{u}(k)\|_p^p.
\end{aligned} \tag{6}
$$

Introducing the "open-loop" error

$$
\boldsymbol{y}_{\text{err,op}}(k+1) = \boldsymbol{y}_{\text{ref}}(k+1) - \boldsymbol{C}\boldsymbol{A}\boldsymbol{x}(k) - \boldsymbol{C}\boldsymbol{B}'\boldsymbol{u}(k-1), \tag{7}
$$

i.e., the error resulting at time-step $k+1$ if no control action is taken at time-step k, (6) takes the form

$$
J_p(k) = \|\boldsymbol{y}_{\text{err,op}}(k+1) - \boldsymbol{C}\boldsymbol{B}'\Delta\boldsymbol{u}(k)\|_p^p + \lambda_u\|\Delta\boldsymbol{u}(k)\|_p^p. \tag{8}
$$

Finally, assuming a two-dimensional output[5], the matrix $\boldsymbol{D} = \boldsymbol{C}\boldsymbol{B} \in \mathbb{R}^{2\times2}$ is (approximately) diagonal[6] with the diagonal elements γ, i.e., $\boldsymbol{D} \approx \text{diag}(\gamma) \succ 0$, and $\succ$ denoting the componentwise inequality [26], (8) can be written as[7]

$$
J_p(k) = \|\boldsymbol{y}_{\text{err,op}}(k+1) - \gamma\boldsymbol{K}\Delta\boldsymbol{u}(k)\|_p^p + \lambda_u\|\Delta\boldsymbol{u}(k)\|_p^p. \tag{9}
$$

Theorem 1. *Consider a power electronic system of the form* (2) *controlled by FCS-MPC given by* (4)*. Direct MPC with the ℓ_1-norm-based objective function* (3) *($p = 1$) can lead to stability issues if $\lambda_u > 0$.*

Proof. For $p = 1$, the objective function (9) becomes

$$
J_1(k) = \|\boldsymbol{y}_{\text{err,op}}(k+1) - \gamma\boldsymbol{K}\Delta\boldsymbol{u}(k)\|_1 + \lambda_u\|\Delta\boldsymbol{u}(k)\|_1. \tag{10}
$$

The solution to the optimization problem (4) strongly depends on the value of the weighting factor $\lambda_u \in \mathbb{R}^+$. Next, we consider the cases $\lambda_u = 0$ and $\lambda_u > 0$ separately.

For $\lambda_u = 0$, the optimization problem can be cast as the integer linear program

$$
\begin{aligned}
&\underset{\boldsymbol{u}(k)\in\mathcal{U}_{\text{adm}}}{\text{minimize}} && \boldsymbol{1}^T\boldsymbol{h} \\
&\text{subject to} && \boldsymbol{h} \succeq \boldsymbol{y}_{\text{err,op}}(k+1) - \gamma\boldsymbol{K}\Delta\boldsymbol{u}(k) \\
& && \boldsymbol{h} \succeq -\big(\boldsymbol{y}_{\text{err,op}}(k+1) - \gamma\boldsymbol{K}\Delta\boldsymbol{u}(k)\big),
\end{aligned} \tag{11}
$$

---

[4]Note that the contribution of the switching effort $\Delta\boldsymbol{u}(k|k)$ is the same regardless of the norm used in (3). As implied by constraint (4d), in each phase switching is allowed by *at most* one step up or down. Therefore, the ℓ_1-norm and the (squared) ℓ_2-norm of the switching transition yield the same cost, i.e., $\|\Delta\boldsymbol{u}(k)\|_1 = \|\Delta\boldsymbol{u}(k)\|_2^2$. For consistency reasons, we use the same norm for the output tracking error and the switching transitions.

[5]To keep the following analysis concise, a two-dimensional output is considered ($n_y = 2$) which can be interpreted as the α- and β-components of the same physical quantity. It is straightforward to show, however, that the arguments made apply to any system described by (2) with an arbitrary number of outputs.

[6]When the forward Euler approximation is used, $\boldsymbol{B} = \boldsymbol{G}T_s$ holds and it is easy to see that $\boldsymbol{D}$ is diagonal. When the exact Euler discretization is employed, the off-diagonal entries of $\boldsymbol{D}$ are nonzero. However, if these elements are several orders of magnitude smaller than the diagonal ones, then they can be neglected without a significant loss of accuracy.

[7]Due to the previously introduced approximation, i.e., $\boldsymbol{D} \approx \text{diag}(\gamma)$, function (9) and all its instances throughout the paper are approximations of (8). With a slight abuse of notation, we use the symbol "$=$" instead of "$\approx$" for simplicity.

---

where $\boldsymbol{1}$ is a vector of appropriate dimension whose components are one, $\boldsymbol{h}$ is a vector of slack variables.

Because there exists always at least one candidate integer solution $\boldsymbol{u}(k) \in \mathcal{U}_{\text{adm}}$ that satisfies the constraints, problem (11) is always feasible. An off-the-self solver, such as a suitable branch-and-bound method, is therefore able to find this solution. The latter is the control action (or switch position) $\boldsymbol{u}^*(k)$ that minimizes the output error. Potential stability issues are avoided and tracking of the output reference trajectories is ensured.

If, on the other hand, $\lambda_u > 0$ holds, the value of the objective function under consideration can be written as

$$
J_1(k) = \begin{cases}
\|\boldsymbol{y}_{\text{err,op}}(k+1)\|_1, & \text{if } \|\Delta\boldsymbol{u}(k)\|_1 = 0 \\
\|\boldsymbol{y}_{\text{err,op}}(k+1) \\
\quad - \gamma\boldsymbol{K}\Delta\boldsymbol{u}(k)\|_1 + c\lambda_u, & \text{if } \|\Delta\boldsymbol{u}(k)\|_1 = c
\end{cases}, \tag{12}
$$

with $c \in \{1, 2, 3\}$. Note that $\|\Delta\boldsymbol{u}(k)\|_1 \in \{0, 1, 2, 3\}$ because of the switching constraint. Therefore, if

$$
\|\boldsymbol{y}_{\text{err,op}}(k+1)\|_1 < \|\boldsymbol{y}_{\text{err,op}}(k+1) - \gamma\boldsymbol{K}\Delta\boldsymbol{u}(k)\|_1 + c\lambda_u, \tag{13}
$$

switching is avoided. This inequality can be rewritten as

$$
\begin{aligned}
\lambda_u > \frac{1}{c}\|\boldsymbol{y}_{\text{err,op}}(k+1)\|_1 &- \frac{1}{c}\|\boldsymbol{y}_{\text{err,op}}(k+1) - \gamma\boldsymbol{K}\Delta\boldsymbol{u}(k)\|_1 \Leftrightarrow \\
\lambda_u > \frac{1}{c}\Big(|y_{\text{err,op},1}(k+1)| &+ |y_{\text{err,op},2}(k+1)| - |y_{\text{err,op},1}(k+1) \\
&- \gamma\boldsymbol{k}_1^T\Delta\boldsymbol{u}(k)| - |y_{\text{err,op},2}(k+1) - \gamma\boldsymbol{k}_2^T\Delta\boldsymbol{u}(k)|\Big),
\end{aligned} \tag{14}
$$

where $\boldsymbol{k}_i^T \in \mathbb{R}^3$, $i = 1, 2$, is the ith row of $\boldsymbol{K}$, and $\boldsymbol{y}_{\text{err,op}} = [y_{\text{err,op},1}\ y_{\text{err,op},2}]^T$.

To investigate the effect of the weighting factor on the stability of the system when the ℓ_1-norm is used, let us assume that

$$
\boldsymbol{y}_{\text{err,op}}(k+1) - \gamma\boldsymbol{K}\Delta\boldsymbol{u}(k) \succeq \boldsymbol{0}_2, \forall \Delta\boldsymbol{u}(k) \in \mathcal{C}_c \tag{15}
$$

with $\boldsymbol{0}_2$ being the 2-dimensional zero vector, and $\mathcal{C}_c = \{\Delta\boldsymbol{u}(k) \mid \|\Delta\boldsymbol{u}(k)\|_1 = c, \|\Delta\boldsymbol{u}(k)\|_\infty = 1\}$. Assumption (15) implies that $\boldsymbol{y}_{\text{err,op}}(k+1) \succeq \boldsymbol{0}_2$, thus we conclude from (14) that

$$
\begin{aligned}
\lambda_u > \frac{1}{c}\Big(y_{\text{err,op},1}(k+1) &+ y_{\text{err,op},2}(k+1) - y_{\text{err,op},1}(k+1) \\
&+ \gamma\boldsymbol{k}_1^T\Delta\boldsymbol{u}(k) - y_{\text{err,op},2}(k+1) + \gamma\boldsymbol{k}_2^T\Delta\boldsymbol{u}(k)\Big) \Leftrightarrow \\
\lambda_u > \frac{\gamma}{c}\Big(\boldsymbol{k}_1^T\Delta\boldsymbol{u}(k) &+ \boldsymbol{k}_2^T\Delta\boldsymbol{u}(k)\Big), \forall \Delta\boldsymbol{u}(k) \in \mathcal{C}_c.
\end{aligned} \tag{16}
$$

Note that according to (16), λ_u is independent of the output open-loop error $\boldsymbol{y}_{\text{err,op}}$.

By following the same procedure as in (16), (15) can be

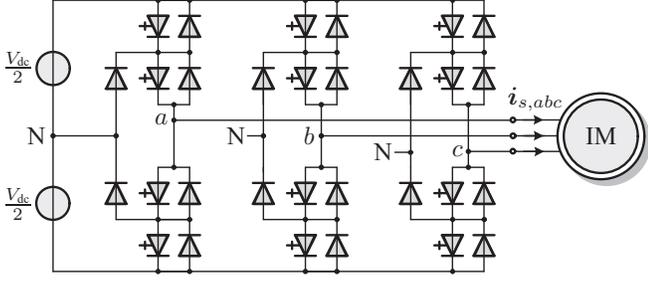Fig. 1. Neutral point clamped (NPC) voltage source inverter driving an induction machine (IM).

(a) Three-phase stator current $\boldsymbol{i}_s$ (solid lines) and their references (dash-dotted lines).

(b) Three-phase switch position $\boldsymbol{u}$.

Fig. 2. Output (stator current) and control action (switch position) when the ℓ_1-norm is used in the objective function and the weighting factor is chosen as $\lambda_u = \lambda_{u,\mathrm{crt}}^{(3)} + \epsilon$.

generalized to

$$
\begin{bmatrix} 1 & 0 \\ 0 & -1 \end{bmatrix} \left(\boldsymbol{y}_{\mathrm{err,op}}(k+1) - \gamma \boldsymbol{K} \Delta \boldsymbol{u}(k) \right) \succeq \boldsymbol{0}_2 \, , \forall \Delta \boldsymbol{u}(k) \in \mathcal{C}_c
$$
$$
\Rightarrow \lambda_u > \frac{\gamma}{c} \left(\boldsymbol{k}_1^T \Delta \boldsymbol{u}(k) - \boldsymbol{k}_2^T \Delta \boldsymbol{u}(k) \right) ,
$$
$$
\begin{bmatrix} -1 & 0 \\ 0 & -1 \end{bmatrix} \left(\boldsymbol{y}_{\mathrm{err,op}}(k+1) - \gamma \boldsymbol{K} \Delta \boldsymbol{u}(k) \right) \succeq \boldsymbol{0}_2 \, , \forall \Delta \boldsymbol{u}(k) \in \mathcal{C}_c
$$
$$
\Rightarrow \lambda_u > \frac{\gamma}{c} \left(-\boldsymbol{k}_1^T \Delta \boldsymbol{u}(k) - \boldsymbol{k}_2^T \Delta \boldsymbol{u}(k) \right) ,
$$
$$
\begin{bmatrix} -1 & 0 \\ 0 & 1 \end{bmatrix} \left(\boldsymbol{y}_{\mathrm{err,op}}(k+1) - \gamma \boldsymbol{K} \Delta \boldsymbol{u}(k) \right) \succeq \boldsymbol{0}_2 \, , \forall \Delta \boldsymbol{u}(k) \in \mathcal{C}_c
$$
$$
\Rightarrow \lambda_u > \frac{\gamma}{c} \left(-\boldsymbol{k}_1^T \Delta \boldsymbol{u}(k) + \boldsymbol{k}_2^T \Delta \boldsymbol{u}(k) \right) . \tag{17}
$$

To find the critical value of λ_u, $\lambda_{u,\mathrm{crt}}^{(c)}$, that simultaneously satisfies conditions (16) and (17) the maximum value of the term within the parentheses must be found for all possible $\Delta \boldsymbol{u}(k) \in \mathcal{C}_c$. To do so, the following problem is solved for each $c \in \{1, 2, 3\}$:[8]

$$
\underset{\boldsymbol{u}(k) \in \mathcal{U}}{\text{maximize}} \quad \|\boldsymbol{K} \Delta \boldsymbol{u}(k)\|_1
$$
$$
\text{subject to} \quad \|\Delta \boldsymbol{u}(k)\|_1 = c \tag{18}
$$
$$
\|\Delta \boldsymbol{u}(k)\|_\infty = 1 \, .
$$

As can be seen, problem (18) is model independent and can be easily solved offline. Having found the solution to (18), i.e., $\Delta \boldsymbol{u}^*(k)$, $\lambda_{u,\mathrm{crt}}^{(c)}$ can be found by setting $\Delta \boldsymbol{u}(k) = \Delta \boldsymbol{u}^*(k)$ in (16) and (17). Based on the resulting critical values
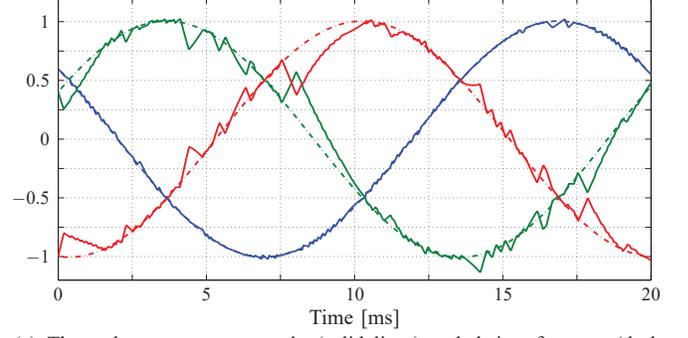
$$
\lambda_{u,\mathrm{crt}}^{(3)} < \lambda_{u,\mathrm{crt}}^{(2)} < \lambda_{u,\mathrm{crt}}^{(1)} , \tag{19}
$$

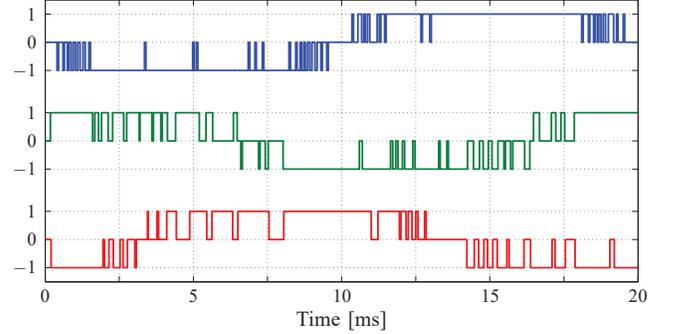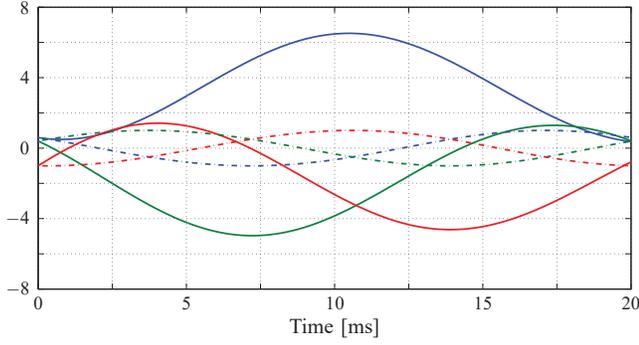the conditions that are necessary and sufficient for (not) switching can be derived. More specifically, if

- $\lambda_{u,\mathrm{crt}}^{(3)} < \lambda_u < \lambda_{u,\mathrm{crt}}^{(2)}$, then simultaneous switching in all three phases is impossible,
- $\lambda_{u,\mathrm{crt}}^{(2)} < \lambda_u < \lambda_{u,\mathrm{crt}}^{(1)}$, then simultaneous switching in two phases is impossible,
- $\lambda_{u,\mathrm{crt}}^{(1)} < \lambda_u$, then switching is avoided altogether. ∎

Example 1. *Consider the drive system shown in Fig. 1 with the parameters stated in Table II. As shown in Section III, the drive model can be written in the form (2). FCS-MPC is employed*

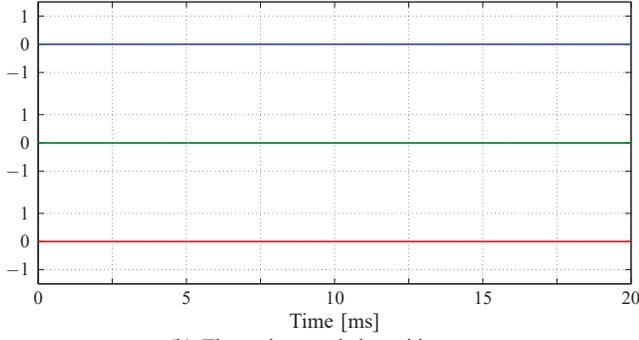[8]A detailed derivation of (18) is provided in Appendix A.

to control the three-phase output (i.e., stator) current of the drive (see Section IV). The closed-loop behavior of this system is shown in Fig. 2 for the weighting factor $\lambda_u = \lambda_{u,crt}^{(3)} + \epsilon$, where $\epsilon > 0$ is an arbitrarily small positive quantity. As can be seen, stability issues arise, because switching transitions that might reduce the output error are prohibited by ruling out simultaneous switching in all three phases[9]. If the value of λ_u is further increased to $\lambda_u = \lambda_{u,crt}^{(1)} + \epsilon$, switching in any of the three phases becomes impossible and the system becomes unstable, see Fig. 3. The outputs fail to track their reference trajectories and the output trajectories evolve according to the natural response of the system.

Note that stability is not guaranteed for $\lambda_u < \lambda_{u,\mathrm{crt}}^{(3)}$. Indeed, the critical values $\lambda_{u,\mathrm{crt}}^{(c)}$ are computed on the basis that (16) and (17) hold *for all* $\Delta \boldsymbol{u}(k) \in \mathcal{C}_c$, thus they provide upper bounds on λ_u. This implies that there exists *some* $\Delta \boldsymbol{u}(k) \in \mathcal{C}_3$ for which switching transitions are avoided under certain conditions for weights that are smaller than their lower critical weight, i.e., for $\lambda_u < \lambda_{u,\mathrm{crt}}^{(3)}$. As λ_u increases and approaches $\lambda_{u,\mathrm{crt}}^{(3)}$, the set of $\Delta \boldsymbol{u}(k)$ that satisfy (16) and (17) becomes larger. Consequently, as $\lambda_u \to \lambda_{u,\mathrm{crt}}^{(3)-}$, i.e., as λ_u approaches $\lambda_{u,\mathrm{crt}}^{(3)}$ from the left, the likelihood that stability problems arise increases.

[9]Note that simultaneously switching in two phases might also be avoided, depending on the total switching cost and the relative tracking error. To better explain the latter, a simple—yet informative—example is discussed in Section V.

(a) Three-phase stator current $\boldsymbol{i}_s$ (solid lines) and their references (dash-dotted lines).

(b) Three-phase switch position $\boldsymbol{u}$.

Fig. 3. Output (stator current) and control action (switch position) when the ℓ_1-norm is used in the objective function and the weighting factor is chosen as $\lambda_u = \lambda_{u,\mathrm{crt}}^{(1)} + \epsilon$.

To this end, consider the following example. We set $c = 3$ and relax assumption (15) so that it is satisfied for some $\Delta\boldsymbol{u}(k) \in \bar{\mathcal{C}}_3 \subset \mathcal{C}_3$ such that $||\boldsymbol{K}\Delta\boldsymbol{u}(k)||_1 < ||\boldsymbol{K}\Delta\boldsymbol{u}^*(k)||_1$. Provided that $\boldsymbol{y}_{\mathrm{err,op}}(k+1) \succeq \boldsymbol{0}_2$ still holds, then $\bar{\lambda}_{u,\mathrm{crt}}^{(3)} < \lambda_{u,\mathrm{crt}}^{(3)}$, where $\bar{\lambda}_{u,\mathrm{crt}}^{(3)}$ is the new λ_u that satisfies (16). By setting $\lambda_u = \bar{\lambda}_{u,\mathrm{crt}}^{(3)}$ switching is avoided, something that would lead to stability problems when $||\boldsymbol{y}_{\mathrm{err,op}}(k+1)||_2 \gg 0$. This issue is exemplified in the following and further discussed in more detail in Section VI when examining the system performance over a wide range of weights λ_u.

Example 2. *Consider the same system and control problem as in Example 1. For the given parameters it results that $\lambda_{u,crt}^{(3)} = 18.1 \cdot 10^{-3}$, see also Section VI. For the present example λ_u is chosen such that $\lambda_u \to \lambda_{u,crt}^{(3)-}$, e.g., $\lambda_u = 18.0 \cdot 10^{-3}$. Assume that at one instant of the problem the state of the system is $\boldsymbol{x}(k) = [0.5696\ 0.8292\ 0.8878\ -0.2158]^T$ (i.e., the output is $\boldsymbol{y}(k) = [0.5696\ 0.8292]^T$) and the desired output value at the next time step is $\boldsymbol{y}_{ref}(k+1) = [0.5906\ 0.8137]^T$. In the sequel two cases are examined depending on the previously applied switch position $\boldsymbol{u}(k-1)$. In the first case assume that it is $\boldsymbol{u}_1(k-1) = [0\ 1\ 0]^T$. Then it is straightforward to show that the optimal switch position is $\boldsymbol{u}_1^*(k) = [1\ 0\ -1]^T$, i.e., all three phases switch to eliminate the error as much as possible. More specifically, the corresponding predicted output is $\boldsymbol{y}(k+1)|_{\boldsymbol{u}_1^*(k)} = [0.5928\ 0.8196]^T$ meaning that $||\ \boldsymbol{y}_{err}(k+1)|_{\boldsymbol{u}_1^*(k)}\ ||_1 = 0.0082$. For the second case*

$\boldsymbol{u}_2(k-1) = [-1\ 1\ 1]^T$. *Ideally, the converter would switch to $\boldsymbol{u}_2(k) = [0\ 0\ 0]^T$ (note that the constraint (4d) limits the feasible options, see also Table I), but this option turns out to be suboptimal. The optimal solution is $\boldsymbol{u}_2^*(k) = [0\ 1\ 0]^T$ which leads to an output of $\boldsymbol{y}(k+1)|_{\boldsymbol{u}_2^*(k)} = [0.5532\ 0.8196]^T$ and thus to an output error of $||\ \boldsymbol{y}_{err}(k+1)|_{\boldsymbol{u}_2^*(k)}\ ||_1 = 0.0434$. Therefore, it can be concluded that depending on $\Delta\boldsymbol{u}(k)$, and as $\lambda_u \to \lambda_{u,crt}^{(3)-}$, switching in all three phases may not always be possible, and consequently potential stability issues may arise.*

Theorem 2. *Consider a power electronic system of the form (2) controlled by FCS-MPC given by (4). Direct MPC with the (squared) ℓ_2-norm in the objective function (3) ($p = 2$) is guaranteed to be stable.*

Proof. For $p = 2$, (9) takes the form

$$J_2(k) = ||\boldsymbol{y}_{\mathrm{err,op}}(k+1) - \gamma\boldsymbol{K}\Delta\boldsymbol{u}(k)||_2^2 + \lambda_u||\Delta\boldsymbol{u}(k)||_2^2. \quad (20)$$

Problem (4) with $J_2(k)$ and $\lambda_u = 0$ is an integer quadratic program that can be solved using a variety of solvers, such as CPLEX [27], Gurobi [28] and MOSEK [29]. Practical stability is guaranteed for FCS-MPC with a prediction horizon of one step provided that the ℓ_2-norm is used in the objective function, as shown in [12].

For $\lambda_u > 0$, and by adopting assumption (15), it follows that

$$\lambda_u > \frac{1}{c}||\boldsymbol{y}_{\mathrm{err,op}}(k+1)||_2^2 - \frac{1}{c}||\boldsymbol{y}_{\mathrm{err,op}}(k+1) - \gamma\boldsymbol{K}\Delta\boldsymbol{u}(k)||_2^2 \Leftrightarrow$$

$$\lambda_u > \frac{1}{c}\Big(||\boldsymbol{y}_{\mathrm{err,op}}(k+1)||_2^2 - ||\boldsymbol{y}_{\mathrm{err,op}}(k+1)||_2^2 - ||\gamma\boldsymbol{K}\Delta\boldsymbol{u}(k)||_2^2$$
$$+ 2\gamma\boldsymbol{y}_{\mathrm{err,op}}^T(k+1)\boldsymbol{K}\Delta\boldsymbol{u}(k)\Big) \Leftrightarrow$$

$$\lambda_u > \frac{\gamma}{c}\Big(-\gamma||\boldsymbol{K}\Delta\boldsymbol{u}(k)||_2^2 + 2\boldsymbol{y}_{\mathrm{err,op}}^T(k+1)\boldsymbol{K}\Delta\boldsymbol{u}(k)\Big),$$
$$\forall \Delta\boldsymbol{u}(k) \in \mathcal{C}_c.$$
$$(21)$$

As can be seen, λ_u depends on $\boldsymbol{y}_{\mathrm{err,op}}(k+1)$. This implies that an upper bound on the λ_u that affects closed-loop stability cannot be derived independently of the open-loop output error at time-step $k+1$. Nevertheless, we observe that for small output errors (i.e., $||\boldsymbol{y}_{\mathrm{err,op}}(k+1)||_2 \approx 0$), small values of λ_u suffice to avoid switching. On the other hand, when $||\boldsymbol{y}_{\mathrm{err,op}}(k+1)||_2 \gg 0$, and for the same λ_u, switching transitions are triggered that ensure stability. This is intuitively clear, since the ℓ_2-norm in the objective function emphasizes large tracking errors, triggering switching transitions to compensate for them.

More formally, (20) can be written as[10]

$$
\begin{aligned}
J_2(k) &= ||\boldsymbol{y}_{\text{err,op}} - \gamma \boldsymbol{K}\Delta\boldsymbol{u}||_2^2 + \lambda_u||\Delta\boldsymbol{u}||_2^2 \\
&= \Delta\boldsymbol{u}^T\gamma^2\boldsymbol{K}^T\boldsymbol{K}\Delta\boldsymbol{u} - 2\gamma\boldsymbol{y}_{\text{err,op}}^T\boldsymbol{K}\Delta\boldsymbol{u} + \lambda_u\Delta\boldsymbol{u}^T\Delta\boldsymbol{u} \\
&\quad + ||\boldsymbol{y}_{\text{err,op}}||_2^2 \\
&= \Delta\boldsymbol{u}^T\underbrace{\left(\gamma^2\boldsymbol{K}^T\boldsymbol{K} + \lambda_u\boldsymbol{I}\right)}_{\boldsymbol{Q}}\Delta\boldsymbol{u} - 2\underbrace{\gamma\boldsymbol{y}_{\text{err,op}}^T\boldsymbol{K}}_{-\boldsymbol{\theta}^T(k+1)}\Delta\boldsymbol{u} \\
&\quad + ||\boldsymbol{y}_{\text{err,op}}||_2^2 \\
&= \Delta\boldsymbol{u}^T\boldsymbol{Q}\Delta\boldsymbol{u} + 2\boldsymbol{\theta}^T\Delta\boldsymbol{u} + \boldsymbol{\theta}^T\boldsymbol{Q}^{-1}\boldsymbol{\theta} \\
&\quad + \underbrace{||\boldsymbol{y}_{\text{err,op}}||_2^2 - \boldsymbol{\theta}^T\boldsymbol{Q}^{-1}\boldsymbol{\theta}}_{\text{const}(k+1)} \\
&= \left(\Delta\boldsymbol{u} + \boldsymbol{Q}^{-1}\boldsymbol{\theta}\right)^T\boldsymbol{Q}\left(\Delta\boldsymbol{u} + \boldsymbol{Q}^{-1}\boldsymbol{\theta}\right) + \text{const} \\
&= ||\Delta\boldsymbol{u} + \boldsymbol{Q}^{-1}\boldsymbol{\theta}||_{\boldsymbol{Q}}^2 + \text{const},
\end{aligned}
\tag{22}
$$

where $\boldsymbol{Q} = \boldsymbol{Q}^T \succ 0$. Therefore, problem (4) with $J_2(k)$ in the form (22) is an integer quadratic program[11] (regardless of the value of λ_u), and thus, as mentioned before, practical stability of the system is guaranteed, according to [12]. Moreover, the same argument can be extended to multistep FCS-MPC, provided that a terminal cost is added to the ℓ_2-norm-based objective function, see [25]. ∎

III. NPC Inverter Drive System Case Study

To demonstrate the impact the choice of norm in the objective function has on the system performance, an industrial case study is considered. More specifically, an MV drive system consisting of a three-phase three-level neutral point clamped (NPC) voltage source inverter is considered. The dc-link voltage V_{dc} is assumed to be constant and the neutral point potential is fixed to zero. As shown in Fig. 1, the inverter drives an induction machine.

At each phase terminal, the NPC inverter can produce the three discrete voltage levels $-\frac{V_{\text{dc}}}{2}$, 0, $\frac{V_{\text{dc}}}{2}$ depending on the position of the four semiconductor switches in the phase leg [30]. To this end, let the integer variable $u_x \in \mathcal{U} = \{-1, 0, 1\}$ denote the switch position in phase $x \in \{a, b, c\}$, which will be manipulated by the controller. Aggregating the switch positions to the input vector $\boldsymbol{u} = [u_a \; u_b \; u_c]^T \in \mathcal{U} = \mathcal{U}^3$, the output voltage of the inverter can be described by

$$
\boldsymbol{v}_{\alpha\beta} = \frac{V_{\text{dc}}}{2}\boldsymbol{u}_{\alpha\beta} = \frac{V_{\text{dc}}}{2}\boldsymbol{K}\boldsymbol{u}.
\tag{23}
$$

The system under consideration can be described by the dynamics of the stator current $\boldsymbol{i}_{s,\alpha\beta}$ and the rotor flux linkage $\boldsymbol{\psi}_{r,\alpha\beta}$. By introducing the state vector $\boldsymbol{x} = [i_{s\alpha} \; i_{s\beta} \; \psi_{r\alpha} \; \psi_{r\beta}]^T \in \mathbb{R}^4$, the continuous-time state equation can be described by (1). By setting $\boldsymbol{y} = \boldsymbol{i}_{s,\alpha\beta} \in \mathbb{R}^2$, we defined the stator current as the system output (or the

[10]In the following derivation, the dependency on the time-step k is dropped to simplify the exposition.

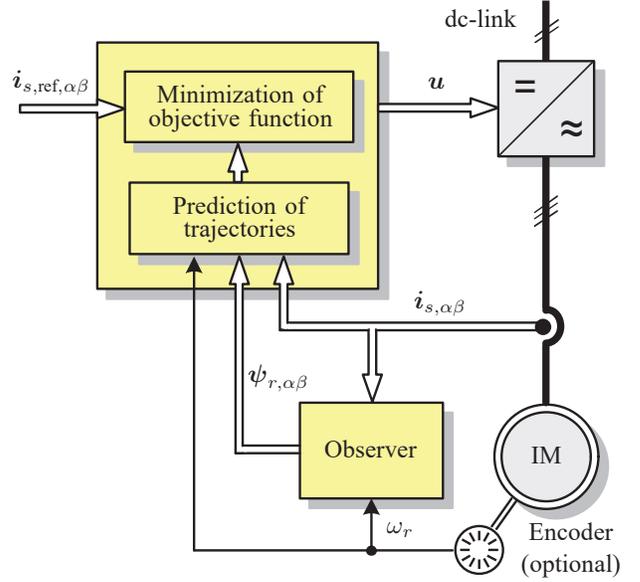[11]Note that the constant term in (22) is independent of $\Delta\boldsymbol{u}(k)$ and can be neglected.

Fig. 4. MPC with current reference tracking for the NPC inverter with an IM.

controlled variable). The matrices $\boldsymbol{F}$, $\boldsymbol{G}$ and $\boldsymbol{C}$—for the specific case study, along with the detailed derivation of the system model, are provided in the Appendix B. Regarding the discrete-time state-space model of the drive, this is of the form (2), where the system matrices are derived using exact Euler discretization.

IV. FCS-MPC with Current Reference Tracking

We consider MPC with current reference tracking, see Fig. 4. The main control objective is the elimination of the current error

$$
\boldsymbol{i}_{s,\text{err},\alpha\beta} = \boldsymbol{i}_{s,\text{ref},\alpha\beta} - \boldsymbol{i}_{s,\alpha\beta},
\tag{24}
$$

which is defined as the difference between the current reference $\boldsymbol{i}_{s,\text{ref},\alpha\beta}$ and the measured stator current. Because switching losses typically dominate over the conduction losses for MV drives, the switching frequency (i.e., the switching effort) has to be kept small. To achieve the latter, as explained in section II, the term $\Delta\boldsymbol{u}(k) = \boldsymbol{u}(k) - \boldsymbol{u}(k-1)$ is penalized.

Switching between $u_x = 1$ and $u_x = -1$ without an intermediate zero switch position has to be prevented in order to avoid a shoot through. To this end, the switching constraint $||\Delta\boldsymbol{u}(k)||_\infty \leq 1$ (see (4d)) is utilized. Depending on $\boldsymbol{u}(k-1)$, this constraint restricts the set of admissible switch positions $\boldsymbol{u}(k) \in \mathcal{U}_{\text{adm}}(k)$ the controller may switch to. For the three-level NPC inverter, the admissible phase switch positions $\mathcal{U}_{\text{adm},x}$ that compose the set of three-phase admissible switch positions $\mathcal{U}_{\text{adm}}(k)$ are summarized in Table I.

Based on the previously stated control objectives, the objective function takes the form

$$
J_p(k) = ||\boldsymbol{i}_{s,\text{err},\alpha\beta}(k+1)||_p^p + \lambda_u||\Delta\boldsymbol{u}(k)||_p^p,
\tag{25}
$$

by setting $\boldsymbol{y}_{\text{err}} = \boldsymbol{i}_{s,\text{err},\alpha\beta}$ in (3). Note that the α- and β-components of the stator current are of the same magnitude,

$u_x(k-1)$	$\mathcal{U}_{\text{adm},x}(k)$
-1	$\{-1, 0\}$
0	$\{-1, 0, 1\}$
1	$\{0, 1\}$

thus the tracking of their reference values is equally emphasized. Moreover, λ_u sets the trade-off between the stator current error and the switching frequency.

To obtain the desired behavior of the drive, the optimal control input $\boldsymbol{u}^*(k)$ that minimizes (25), is computed. To do so, the stator current at time step $k+1$ is predicted based on (2). This is done for all admissible $\boldsymbol{u}(k) \in \boldsymbol{\mathcal{U}}_{\text{adm}}(k)$ that meet the switching constraint. Therefore, the optimization problem to be solved is of the form (4), where function (4a) is given by (25).

V. IMPACT OF THE CHOICE OF NORM: DISCUSSION

To exemplify the effect of the norm used in the objective function (25), two possible instances of the optimization problem (4) are presented. In both cases, the previously applied input is $\boldsymbol{u}(k-1) = [0\ 0\ 0]^T$, thus the set of admissible switch positions at time-step k is $\boldsymbol{\mathcal{U}}_{\text{adm}}(k) = \boldsymbol{\mathcal{U}}$. This implies that all of the $3^3 = 27$ switch positions $\boldsymbol{u}(k)$ need to be evaluated to determine the optimal one. Nonetheless, for the sake of simplicity—but without loss of generality—only three out of the 27 candidate solutions are examined in the following examples, labeled as $\boldsymbol{u}_0(k)$, $\boldsymbol{u}_1(k)$ and $\boldsymbol{u}_2(k)$. The three-phase switch position $\boldsymbol{u}_0(k)$ is chosen as $\boldsymbol{u}_0(k) = \boldsymbol{u}(k-1)$, whereas the other two three-phase switch positions incur one switching transition, i.e., $\|\Delta\boldsymbol{u}_z(k)\| = 1$, $\forall \boldsymbol{u}_z(k), z \in \{1, 2\}$. Finally, to further simplify the exposition, we assume that all three examined switch positions have approximately the same influence on the tracking error in the β-axis regardless of the norm used, i.e., $\left|i_{s,\text{err},\beta}(k+1)\big|_{\boldsymbol{u}_z(k)}\right| \approx \left(i_{s,\text{err},\beta}(k+1)\big|_{\boldsymbol{u}_z(k)}\right)^2$, $\forall \boldsymbol{u}_z(k)$, $z \in \{0, 1, 2\}$. This implies that the contribution of the β-component of the current error to the overall cost can be interpreted as merely an offset, thus it can be discarded without affecting the analysis presented hereafter. Hence, we restrict our discussion to the α-axis.

For the first instance examined, the current error in the α-axis at time-step k is small, i.e., $|i_{s,\text{err},\alpha}(k)| \approx 0$, see Fig. 5(a). As can be seen in this figure, the predicted current can take three possible values at time-step $k + 1$ depending on the three examined switch positions $\boldsymbol{u}(k)$, i.e., $i_{s,\alpha}(k+1)\big|_{\boldsymbol{u}_0(k)}$, $i_{s,\alpha}(k+1)\big|_{\boldsymbol{u}_1(k)}$, and $i_{s,\alpha}(k+1)\big|_{\boldsymbol{u}_2(k)}$. The resulting values of $J_1(k)$ (i.e., with the ℓ_1-norm) are depicted in Fig. 5(b). The black bar shows the contribution of the current error term, i.e., the tracking error cost, which depends linearly on the current error $i_{s,\text{err},\alpha}(k)$. The gray bar indicates the contribution of the switching effort term, i.e., the switching cost. On the other hand, when the (squared) ℓ_2-norm ($p = 2$) is used in
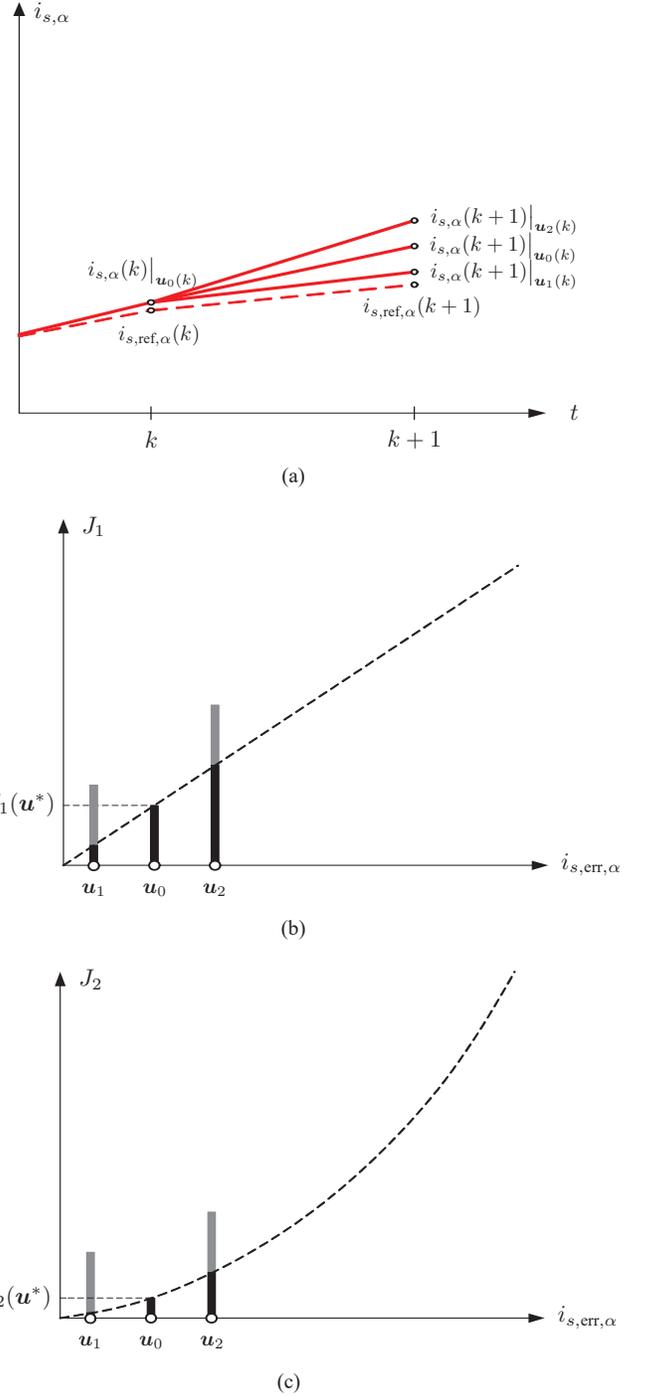

Fig. 5. Impact of the choice of norm on the selection of the switch position when the current error is small. (a) Instance of the problem. (b) Penalization of the current error and the switching effort based on the ℓ_1-norm. (c) Penalization of the current error and the switching effort based on the (squared) ℓ_2-norm. The switching cost is shown with the gray bar and the tracking error with the black bar.

the objective function (25), the tracking error cost changes quadratically with the current error, see Fig. 5(c).

As can be observed in Fig. 5(a), the predicted α-axis current at $k + 1$ deviates the most from the current reference when

$\boldsymbol{u}_2(k)$ is applied, because

$$
\begin{aligned}
\left\| i_{s,\mathrm{err},\alpha}(k+1)\big|_{\boldsymbol{u}_1(k)} \right\|_p^p &< \left\| i_{s,\mathrm{err},\alpha}(k+1)\big|_{\boldsymbol{u}_0(k)} \right\|_p^p \\
&< \left\| i_{s,\mathrm{err},\alpha}(k+1)\big|_{\boldsymbol{u}_2(k)} \right\|_p^p .
\end{aligned}
\tag{26}
$$

The option $\boldsymbol{u}_2(k)$ is consequently suboptimal and is thus not further discussed. As for the remaining two options, $\boldsymbol{u}_0(k)$ and $\boldsymbol{u}_1(k)$, the controller will refrain from switching for both norms, because the switching cost dominates over the tracking error cost. In other words, because

$$
\left| i_{s,\mathrm{err},\alpha}(k+1)\big|_{\boldsymbol{u}_0(k)} \right| < \lambda_u \quad \text{and}
$$

$$
\left(i_{s,\mathrm{err},\alpha}(k+1)\big|_{\boldsymbol{u}_0(k)} \right)^2 < \lambda_u
$$

hold, keeping the old switch position yields the minimal cost and is thus optimal.

Fig. 6(a) depicts the same situation as before, with the difference that a large current error occurs at time-step k, i.e., $|i_{s,\mathrm{err},\alpha}(k)| \gg 0$. As before, (26) holds, thus the option $\boldsymbol{u}_2(k)$ can be easily excluded. However, the choice between $\boldsymbol{u}_0(k)$ and $\boldsymbol{u}_1(k)$ depends on the norm used in the objective function. More specifically, when the ℓ_1-norm is used and

$$
\left| i_{s,\mathrm{err},\alpha}(k+1)\big|_{\boldsymbol{u}_0(k)} \right| < \left| i_{s,\mathrm{err},\alpha}(k+1)\big|_{\boldsymbol{u}_1(k)} \right| + \lambda_u
$$

holds, then the controller concludes that $\boldsymbol{u}^*(k) = \boldsymbol{u}_0(k) = \boldsymbol{u}(k-1)$ is the optimal solution to (4); a switching transition, which could reduce the current error, is not triggered. In other words, when the switching cost (gray bar in Fig. 6(b)) outweighs the *relative* reduction in the tracking error, as defined by the difference $\left| i_{s,\mathrm{err},\alpha}(k+1)\big|_{\boldsymbol{u}_0(k)} \right| - \left| i_{s,\mathrm{err},\alpha}(k+1)\big|_{\boldsymbol{u}_1(k)} \right|$, then switching is avoided regardless of the *absolute* tracking error. As a result, the current error increases, the controller tracking performance deteriorates and stability issues arise.

On the other hand, when the (squared) ℓ_2-norm is used and

$$
\left(i_{s,\mathrm{err},\alpha}(k+1)\big|_{\boldsymbol{u}_0(k)} \right)^2 > \left(i_{s,\mathrm{err},\alpha}(k+1)\big|_{\boldsymbol{u}_1(k)} \right)^2 + \lambda_u
$$

holds, i.e., the difference between the predicted squared current errors for $\boldsymbol{u}_0(k)$ and $\boldsymbol{u}_1(k)$ exceeds the switching cost, then a switching transition occurs from $\boldsymbol{u}(k-1)$ to $\boldsymbol{u}_1(k)$ to reduce the current error. This is indicated in Fig. 6(c). Consequently, and as shown in [12], closed-loop stability is ensured.

VI. PERFORMANCE EVALUATION

The simulation results presented in this section relate to the MV drive system depicted in Fig. 1. The inverter is fed by the constant dc-link voltage $V_{\mathrm{dc}} = 5.2\,\mathrm{kV}$ and a fixed neutral point potential N. A $3.3\,\mathrm{kV}$, $356\,\mathrm{A}$ and $50\,\mathrm{Hz}$ squirrel-cage induction machine rated at $2\,\mathrm{MVA}$, with $596\,\mathrm{rpm}$ nominal rotational speed and a 0.25 p.u. total leakage inductance is used. The rated values of the induction machine and the parameters of the drive are summarized in Table II both in SI quantities and in the p.u. system. According to the objective function (25), the one-step horizon case is investigated. The behavior of the
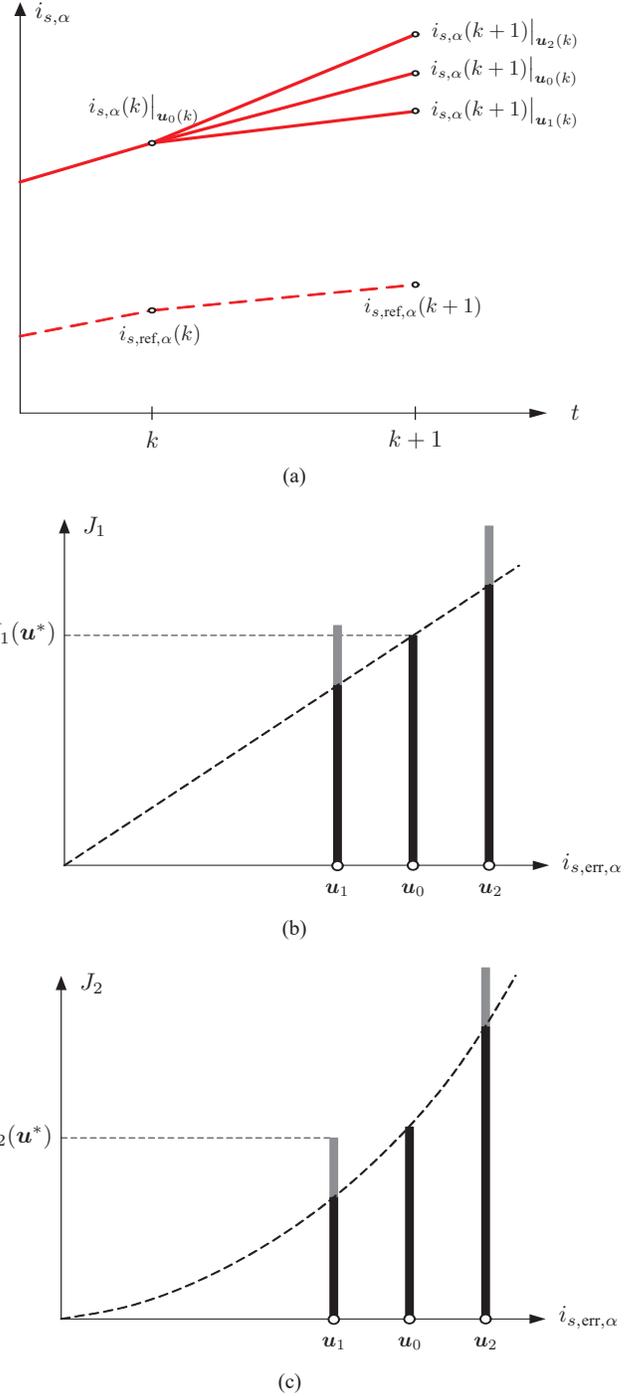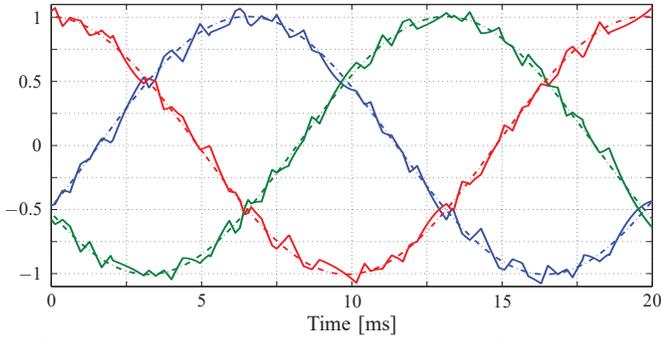

Fig. 6. Impact of the choice of norm on the selection of the switch position when the current error is large. (a) Instance of the problem. (b) Penalization of the current error and the switching effort based on the ℓ_1-norm. (c) Penalization of the current error and the switching effort based on the (squared) ℓ_2-norm. The switching cost is shown with the gray bar and the tracking error with the black bar.

drive system is examined for the ℓ_2-norm and the ℓ_1-norm. The sampling interval $T_s = 25\,\mu\mathrm{s}$ is used.
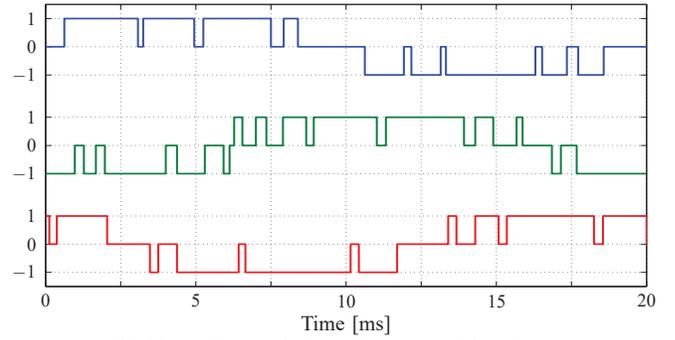
1) Objective Function With the ℓ_2-Norm: First, the steady-state performance of the system is examined when using the (squared) ℓ_2-norm in (25), i.e., $p = 2$. The weighting factor is set to $\lambda_u = 2.5 \cdot 10^{-3}$, which results in an average switching frequency per semiconductor device of $f_{\mathrm{sw}} = 268\,\mathrm{Hz}$. The

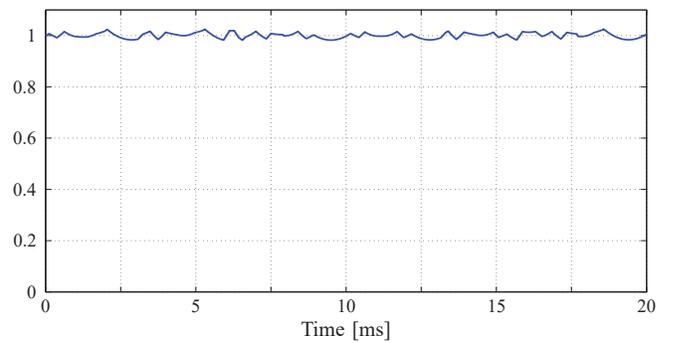| Rated values		Parameters	
		Induction Motor	
Voltage	3.3 kV	Stator resistance (R_s)	57.61 mΩ (0.0108 p.u.)
Current	356 A	Rotor resistance (R_r)	48.89 mΩ (0.0091 p.u.)
Real power	1.587 MW	Stator leakage reactance (X_{ls})	2.544 mH (0.1493 p.u.)
Apparent power	2.035 MVA	Rotor leakage reactance (X_{lr})	1.881 mH (0.1104 p.u.)
Stator frequency	50 Hz	Mutual reactance (X_m)	40.01 mH (2.349 p.u.)
Rotational speed	596 rpm		
		Inverter	
		Dc-link voltage (V_{dc})	5.2 kV (1.930 p.u.)

(a) Three-phase stator current i_s (solid lines) and their references (dash-dotted lines).

(b) Three-phase switch position (control input) u.

(c) Electromagnetic torque T_e (solid line) and its reference (dash-dotted line).

(d) Stator flux magnitude Ψ_s.

Fig. 7. Simulated waveforms produced by the direct model predictive controller with current reference tracking during steady-state operation, at full speed and rated torque. The (squared) ℓ_2-norm and the weighting factor $\lambda_u = 2.5 \cdot 10^{-3}$ are used in the objective function.

simulation results for this scenario are shown in Fig. 7. As can be seen in Fig. 7(a), the three-phase stator currents (solid lines), which are shown for one fundamental period, accurately track their references (dash-dotted lines). The low switching frequency and the short horizon of one time step, though, lead to relatively high current ripples and to the current total harmonic distortion (THD) of $I_{\text{THD}} = 5.84\%$. Fig. 7(b) shows the three-phase switch positions, while the electromagnetic torque and the magnitude of the stator flux are depicted in Figs. 7(c) and 7(d), respectively. Based on these results, it can be concluded that the steady-state performance of the drive is relatively good.

In a next step, the weighting factor λ_u is varied in order to investigate the trade-off between the current THD and the average switching frequency. The resulting current THD and the switching frequency are shown for $0 \leq \lambda_u \leq 0.02$ in Figs. 8(a) and 8(b), respectively. As can be observed in Fig. 8(a), the current THD depends almost linearly on λ_u for $\lambda_u \leq 0.017$. The switching frequency decreases steeply from its peak at 3440 Hz for $\lambda_u = 0$ to about 70 Hz at $\lambda_u = 0.0175$, as shown in the log-linear plot in Fig. 8(b). For $\lambda_u \geq 0.018$, six-step operation is reached, implying a switching frequency of 50 Hz. The current THD is about 20%.

A useful performance metric that characterizes the control scheme is the product of the current distortions and the device
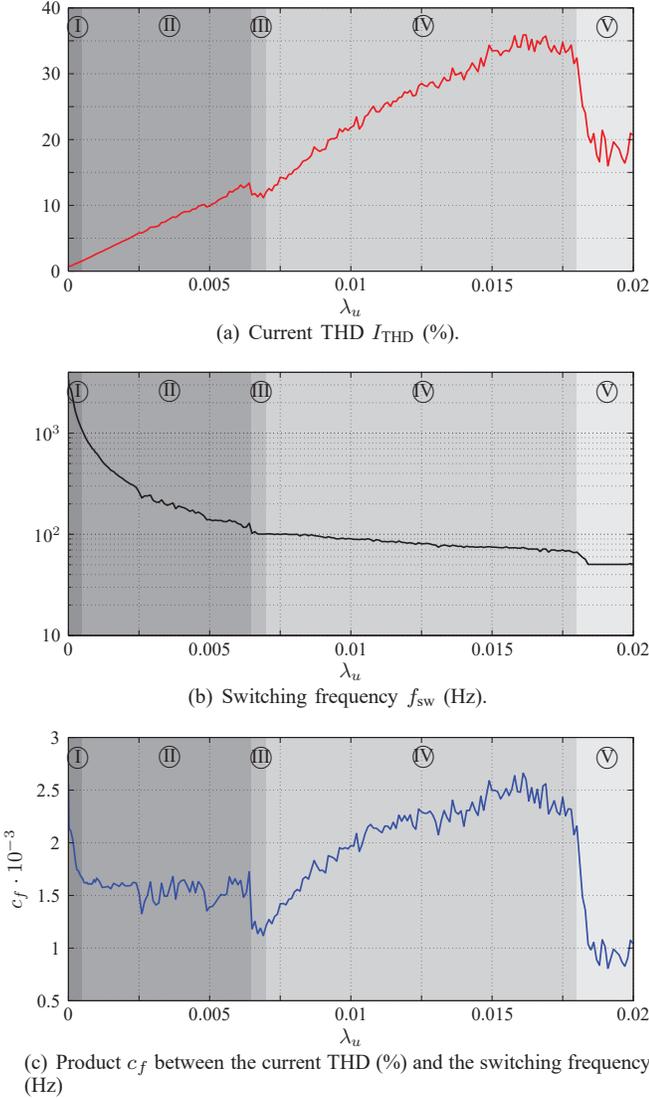
(a) Current THD I_{THD} (%).

(b) Switching frequency f_{sw} (Hz).

(c) Product c_f between the current THD (%) and the switching frequency (Hz)

Fig. 8. Trade-off curves when the ℓ_2-norm is used in the objective function. The current THD, switching frequency and the product of the two scaled by 1000 are shown as a function of the weighting factor λ_u.

switching frequency, i.e.,

$$c_f = I_{\text{THD}} \cdot f_{\text{sw}}. \tag{27}$$

As shown for example in [31], c_f is effectively a constant for control schemes based on pulse width modulation (PWM). For the discussed direct MPC strategy, however, this is not the case.

Indeed, roughly five distinct regions governed by different characteristics can be observed in Fig. 8(c). For three of them, i.e., $0.0005 \leq \lambda_u < 0.0065$ (region II), $0.0065 \leq \lambda_u < 0.007$ (region III) and $\lambda_u \geq 0.018$ (region V), the ratio between current distortions and switching frequency is favorable, because c_f is below 1600 and thus relatively small. More specifically, in region II, the switching frequency is between 100 Hz and 1 kHz, c_f is approximately 1600 and the current THD changes linearly with λ_u. Considering that an MV drive typically operates within this range of switching frequencies, the tuning of the controller is relative simple. The metric c_f is very

low (≈ 1100) in region III and the switching frequency is constant and equal to 100 Hz. Finally, in six-step operation (region V), c_f attains its lowest value of approximately 1000, implying that even for that range of values of λ_u, the system performance is acceptable.

On the other hand, in the two remaining regions $\lambda_u < 0.0005$ (region I) and $0.007 \leq \lambda_u < 0.018$ (region IV), the values of c_f are mostly high, indicating an unfavorable ratio between current distortions and switching frequency. In region I, in which the switching penalty is close to zero, the switching frequency increases disproportionately; large increases in the switching frequency lead to only minor reductions in the current THD. Finally, the same unfavorable behavior is observed in region IV, where the drive operates at very low switching frequencies between 70 and 100 Hz.

2) Objective Function With the ℓ_1-Norm: Operating under the same conditions as before, the steady-state performance of the drive is examined when the ℓ_1-norm is used. The weighting factor is chosen as $\lambda_u = 16 \cdot 10^{-3}$ and the resulting average switching frequency is $f_{\text{sw}} = 1266\,\text{Hz}$. For the given system parameters (see Table II), the critical weights $\lambda_{u,\text{crt}}^{(3)} = 18.1 \cdot 10^{-3}$, $\lambda_{u,\text{crt}}^{(2)} = 23.6 \cdot 10^{-3}$ and $\lambda_{u,\text{crt}}^{(1)} = 27.1 \cdot 10^{-3}$ result. The resulting waveforms of the stator currents, the three-phase switch positions, the electromagnetic torque and the magnitude of the stator flux are shown in Fig. 9. Despite the relatively high switching frequency, large current errors occur resulting in torque deviations from its reference value of more than 30%, see Figs. 9(a) and 9(c), respectively. It can be concluded that the system becomes temporarily unstable, which clearly deteriorates the overall closed-loop performance. Based on the analysis given in Section II, this behavior of the system is expected considering that $\lambda_u \to \lambda_{u,\text{crt}}^{(3)-}$.

For a final comparison between the ℓ_1- and the ℓ_2-norm, λ_u is again varied between 0 and 0.02. The resulting current THD and switching frequency are recorded and shown in Fig. 10. As can be seen for $\lambda_u < 0.0072$ (region I), the switching frequency and the current THD are almost constant. For $0.0072 \leq \lambda_u < 0.0198$ (region II), however, the switching frequency decreases in a somewhat linear manner (it remains, though, above 1 kHz), causing a gradual increase in the current THD; a stepwise increase occurs for $\lambda_u > 0.0171$, i.e., as λ_u approaches $\lambda_{u,\text{crt}}^{(3)}$. For $\lambda_u \geq 0.0198$ (region III), i.e., for $\lambda_{u,\text{crt}}^{(3)} < \lambda_u < \lambda_{u,\text{crt}}^{(2)}$, the switching frequency approaches zero, the tracking of the current is lost and the system becomes unstable. Based on these observations, it can be concluded that the ℓ_1-norm is an unfortunate choice for two reasons. The controller is effective only for a very limited range of values of λ_u and it fails to meet the second control objective, i.e., the operation at switching frequencies of a few hundred Hz.

VII. CONCLUSIONS

The choice of norm has a profound impact on the closed-loop system performance when direct model predictive control (MPC) with reference tracking is employed. Despite the common belief that an objective function with the ℓ_1-norm is preferable for computational simplicity, the ℓ_1-norm is a poor

(a) Three-phase stator current i_s (solid lines) and their references (dash-dotted lines).

(b) Three-phase switch position (control input) u.

(c) Electromagnetic torque T_e (solid line) and its reference (dash-dotted line).
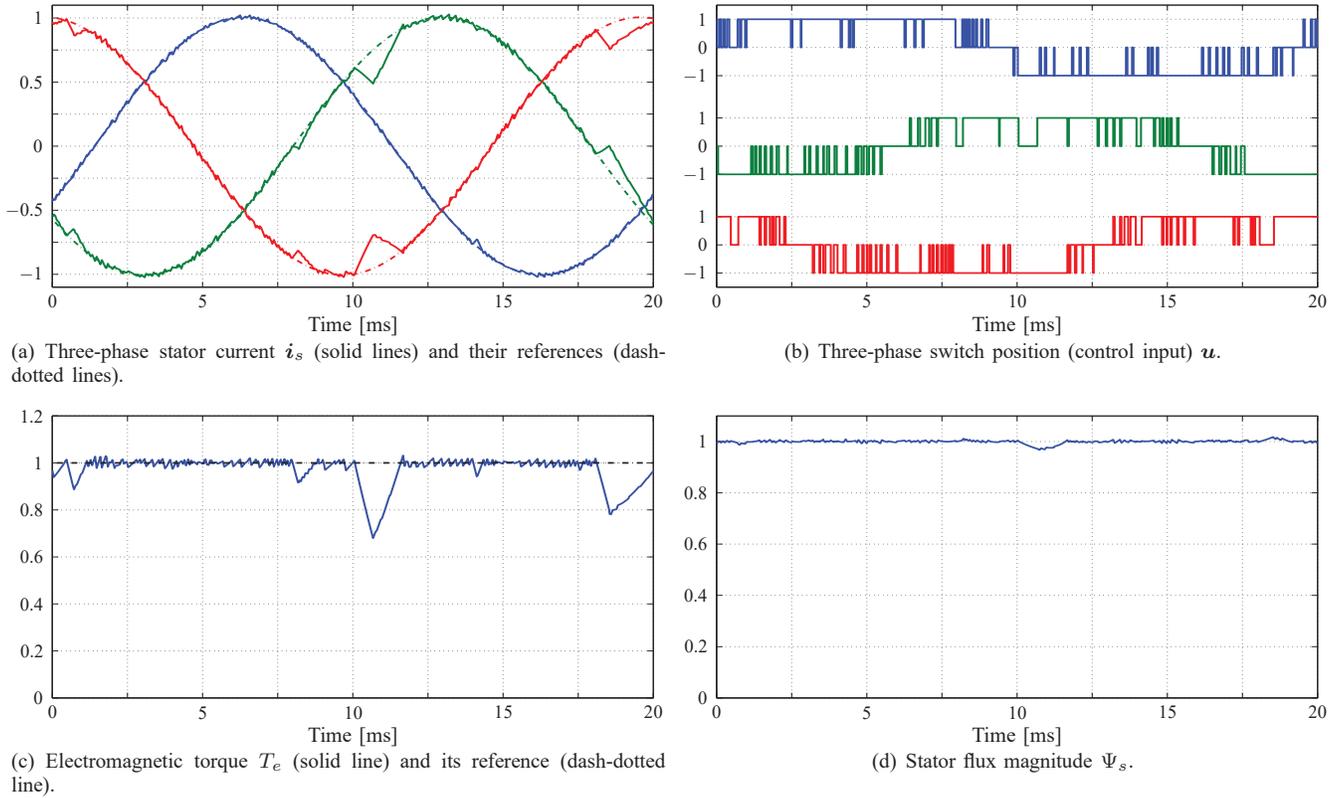
(d) Stator flux magnitude Ψ_s.

Fig. 9. Simulated waveforms produced by the direct model predictive controller with current reference tracking during steady-state operation, at full speed and rated torque. The ℓ_1-norm and the weighting factor $\lambda_u = 16 \cdot 10^{-3}$ are used in the objective function.

(a) Current THD I_{THD} (%).
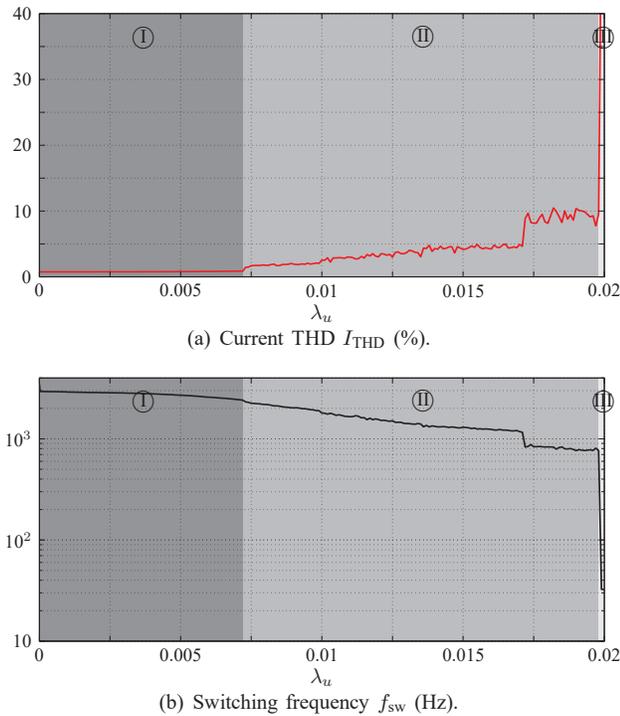
(b) Switching frequency f_{sw} (Hz).

Fig. 10. Trade-off curves when the ℓ_1-norm is used in the objective function. The current THD and the switching frequency are shown as a function of the weighting factor λ_u.

choice. Operation at low switching frequencies is impaired,

tuning is difficult and stability issues arise. As was proven in this paper, for penalties on the switching effort in excess of $\lambda_{u,\mathrm{crt}}^{(1)}$, the controller with a horizon of $N = 1$ and the ℓ_1-norm for a linear system with integer inputs stops operating altogether. The (squared) ℓ_2-norm avoids these issues and is thus clearly preferable. In particular, the ℓ_2-norm guarantees closed-loop stability, see [12].

This paper presented and analyzed the impact of the choice of norm in depth and used an industrial case study to verify the theoretical analysis. To this end, a three-level inverter drive system was used to illustrate and confirm the issues associated with the ℓ_1-norm and the benefit of adopting the ℓ_2-norm in the objective function.

APPENDIX A
CALCULATION OF THE CRITICAL VALUE OF λ_u

The critical value of λ_u is that value that simultaneously satisfies all four inequalities in (16) and (17). Thus, the λ_u that is *always* greater than all four left-hand sides is that $\lambda_{u,\mathrm{crt}}^{(c)} > 0$ that is greater than the maximum possible values of the dot products formed by the matrix-vector multiplication $K\Delta u(k)$ for all $\Delta u(k) \in \mathcal{C}_c$ (note that the constant factor γ/c does not affect the optimal value, and thus it can be neglected). To find the maximum value resulting by the aforementioned multiplication $K\Delta u(k)$ one has to take into account the absolute values of the dot products, i.e., the ℓ_1-norm of the product is required.

Finally, to find the feasible $\lambda_{u,\mathrm{crt}}^{(c)}$, the formulated objective function $||K\Delta u(k)||_1$ is minimized, subject to the constraints

imposed according to the definition of $\mathcal{C}_c$, i.e., the feasible set. As a result, the optimization problem that computes $\lambda_{u,\text{crt}}^{(c)}$ takes the form (18).

APPENDIX B
CONTINUOUS-TIME MODEL OF THE DRIVE SYSTEM

According to (23)—and considering that there are $3^3 = 27$ different vectors of the form $\boldsymbol{u} = [u_a \ u_b \ u_c]^T$—the inverter unit can produce 19 unique voltage vectors $\boldsymbol{v}_{\alpha\beta}$ in the $\alpha\beta$-plane. The output voltage of the inverter is the voltage applied to the stator windings of the machine.

Before deriving the state-space model of the squirrel-cage induction machine in the $\alpha\beta$-plane, it should be mentioned that the dynamic of the rotor angular speed ω_r is neglected, since the speed is considered to be a time-varying parameter. As mentioned in Section III, the stator current $\boldsymbol{i}_{s,\alpha\beta}$ and the rotor flux vector $\boldsymbol{\psi}_{r,\alpha\beta}$ are the state variables. Moreover, the machine input is the stator voltage $\boldsymbol{v}_{s,\alpha\beta}$, which is equal to the inverter output voltage, as given by (23). The model parameters are the stator and rotor resistances R_s and R_r, respectively, the stator, rotor and mutual reactances X_{ls}, X_{lr} and X_m, respectively, the inertia M, and the mechanical load torque T_ℓ.

Considering the above, the continuous-time state equations are[12] [32]

$$\frac{d\boldsymbol{i}_s}{dt} = -\frac{1}{\tau_s}\boldsymbol{i}_s + \left(\frac{1}{\tau_r}\boldsymbol{I} - \omega_r\begin{bmatrix} 0 & -1 \\ 1 & 0 \end{bmatrix}\right)\frac{X_m}{\Phi}\boldsymbol{\psi}_r + \frac{X_r}{\Phi}\boldsymbol{v}_s$$
(28a)

$$\frac{d\boldsymbol{\psi}_r}{dt} = \frac{X_m}{\tau_r}\boldsymbol{i}_s - \frac{1}{\tau_r}\boldsymbol{\psi}_r + \omega_r\begin{bmatrix} 0 & -1 \\ 1 & 0 \end{bmatrix}\boldsymbol{\psi}_r$$
(28b)

$$\frac{d\omega_r}{dt} = \frac{1}{M}(T_e - T_\ell)$$
(28c)

with $\Phi = X_sX_r - X_m^2$, $X_s = X_{ls} + X_m$ and $X_r = X_{lr} + X_m$. Furthermore, we define $\tau_s = X_r\Phi/(R_sX_r^2 + R_rX_m^2)$ and $\tau_r = X_r/R_r$ as the transient stator and rotor time constants, respectively. $\boldsymbol{I}$ is the identity matrix of appropriate dimension (here two by two), whereas T_e is the electromagnetic torque, which is given by

$$T_e = \frac{X_m}{X_r}(\psi_{r\alpha}i_{s\beta} - \psi_{r\beta}i_{s\alpha}).$$
(29)

Combining (23) and (28), the state-space model of the drive system in the continuous-time domain can be written in the form (1). The matrices $\boldsymbol{F}$, $\boldsymbol{G}$, and $\boldsymbol{C}$ are

$$\boldsymbol{F} = \begin{bmatrix} -\frac{1}{\tau_s} & 0 & \frac{X_m}{\tau_r\Phi} & \omega_r\frac{X_m}{\Phi} \\ 0 & -\frac{1}{\tau_s} & -\omega_r\frac{X_m}{\Phi} & \frac{X_m}{\tau_r\Phi} \\ \frac{X_m}{\tau_r} & 0 & -\frac{1}{\tau_r} & -\omega_r \\ 0 & \frac{X_m}{\tau_r} & \omega_r & -\frac{1}{\tau_r} \end{bmatrix}, \ \boldsymbol{G} = \frac{X_r}{\Phi}\frac{V_{dc}}{2}\begin{bmatrix} 1 & 0 \\ 0 & 1 \\ 0 & 0 \\ 0 & 0 \end{bmatrix},$$

$$\boldsymbol{C} = \begin{bmatrix} 1 & 0 & 0 & 0 \\ 0 & 1 & 0 & 0 \end{bmatrix}.$$

[12]In (28), all vectors are given in the $\alpha\beta$-plane and the subscripts are dropped for convenience.

REFERENCES

[1] J. M. Maciejowski, *Predictive Control with Constraints*. Englewood Cliffs, NJ: Prentice-Hall, 2002.

[2] J. B. Rawlings and D. Q. Mayne, *Model Predictive Control: Theory and Design*. Madison, WI: Nob Hill, 2009.

[3] C. E. García, D. M. Prett, and M. Morari, "Model predictive control: Theory and practice—A survey," *Automatica*, vol. 25, no. 3, pp. 335–348, Mar. 1989.

[4] D. Q. Mayne, J. B. Rawlings, C. V. Rao, and P. O. M. Scokaert, "Constrained model predictive control: Stability and optimality," *Automatica*, vol. 36, no. 6, pp. 789–814, Jun. 2000.

[5] A. Linder and R. Kennel, "Model predictive control for electrical drives," in *Proc. IEEE Power Electron. Spec. Conf.*, Recife, Brazil, Jun. 2005, pp. 1793–1799.

[6] T. Geyer, G. Papafotiou, and M. Morari, "Model predictive control in power electronics: A hybrid systems approach," in *Proc. IEEE Conf. Decis. Control*, Seville, Spain, Dec. 2005, pp. 5606–5611.

[7] P. Cortés, M. P. Kazmierkowski, R. M. Kennel, D. E. Quevedo, and J. Rodríguez, "Predictive control in power electronics and drives," *IEEE Trans. Ind. Electron.*, vol. 55, no. 12, pp. 4312–4324, Dec. 2008.

[8] J. Rodríguez, M. P. Kazmierkowski, J. R. Espinoza, P. Zanchetta, H. Abu-Rub, H. A. Young, and C. A. Rojas, "State of the art of finite control set model predictive control in power electronics," *IEEE Trans. Ind. Informat.*, vol. 9, no. 2, pp. 1003–1016, May 2013.

[9] S. Vazquez, J. I. Leon, L. G. Franquelo, J. Rodríguez, H. A. Young, A. Marquez, and P. Zanchetta, "Model predictive control: A review of its applications in power electronics," *IEEE Ind. Electron. Mag.*, vol. 8, no. 1, pp. 16–31, Mar. 2014.

[10] J. Rodríguez, J. Pontt, C. A. Silva, P. Correa, P. Lezana, P. Cortés, and U. Ammann, "Predictive current control of a voltage source inverter," *IEEE Trans. Ind. Electron.*, vol. 54, no. 1, pp. 495–503, Feb. 2007.

[11] P. Cortés, A. Wilson, S. Kouro, J. Rodríguez, and H. Abu-Rub, "Model predictive control of cascaded H-bridge multilevel inverters," *IEEE Trans. Ind. Electron.*, vol. 57, no. 8, pp. 2691–2699, Aug. 2010.

[12] R. P. Aguilera and D. E. Quevedo, "Predictive control of power converters: Designs with guaranteed performance," *IEEE Trans. Ind. Informat.*, vol. 11, no. 1, pp. 53–63, Feb. 2015.

[13] P. Cortés, J. Rodríguez, P. Antoniewicz, and M. Kazmierkowski, "Direct power control of an AFE using predictive control," *IEEE Trans. Power Electron.*, vol. 23, no. 5, pp. 2516–2523, Sep. 2008.

[14] S. Vazquez, A. Marquez, R. Aguilera, D. Quevedo, J. I. Leon, and L. G. Franquelo, "Predictive optimal switching sequence direct power control for grid-connected power converters," *IEEE Trans. Ind. Electron.*, vol. 62, no. 4, pp. 2010–2020, Apr. 2015.

[15] T. Geyer, G. Papafotiou, R. Frasca, and M. Morari, "Constrained optimal control of the step-down dc-dc converter," *IEEE Trans. Power Electron.*, vol. 23, no. 5, pp. 2454–2464, Sep. 2008.

[16] P. Karamanakos, T. Geyer, and S. Manias, "Direct voltage control of dc-dc boost converters using enumeration-based model predictive control," *IEEE Trans. Power Electron.*, vol. 29, no. 2, pp. 968–978, Feb. 2014.

[17] P. Correa, M. Pacas, and J. Rodríguez, "Predictive torque control for inverter-fed induction machines," *IEEE Trans. Ind. Electron.*, vol. 54, no. 2, pp. 1073–1079, Apr. 2007.

[18] T. Geyer, G. Papafotiou, and M. Morari, "Model predictive direct torque control—Part I: Concept, algorithm and analysis," *IEEE Trans. Ind. Electron.*, vol. 56, no. 6, pp. 1894–1905, Jun. 2009.

[19] T. Geyer, "Computationally efficient model predictive direct torque control," *IEEE Trans. Power Electron.*, vol. 26, no. 10, pp. 2804–2816, Oct. 2011.

[20] T. Geyer and D. E. Quevedo, "Multistep finite control set model predictive control for power electronics," *IEEE Trans. Power Electron.*, vol. 29, no. 12, pp. 6836–6846, Dec. 2014.

[21] T. Geyer, N. Oikonomou, G. Papafotiou, and F. D. Kieferndorf, "Model predictive pulse pattern control," *IEEE Trans. Ind. Appl.*, vol. 48, no. 2, pp. 663–676, Mar./Apr. 2012.

[22] T. Geyer, P. Karamanakos, and R. Kennel, "On the benefit of long-horizon direct model predictive control for drives with LC filters," in *Proc. IEEE Energy Convers. Congr. Expo.*, Pittsburgh, PA, Sep. 2014, pp. 3520–3527.

[23] T. Geyer and D. E. Quevedo, "Performance of multistep finite control set model predictive control for power electronics," *IEEE Trans. Power Electron.*, vol. 30, no. 3, pp. 1633–1644, Mar. 2015.

[24] J. Rodríguez and P. Cortés, *Predictive control of power converters and electrical drives*. Chichester, UK: Wiley, 2012.

[25] R. P. Aguilera and D. E. Quevedo, "Stability analysis of quadratic MPC with a discrete input alphabet," *IEEE Trans. Autom. Control*, vol. 58, no. 12, pp. 3190–3196, Dec. 2013.

[26] S. Boyd and L. Vandenberghe, *Convex Optimization*. Cambridge, UK: Cambridge Univ. Press, 2004.

[27] IBM ILOG, Inc., *CPLEX optimizer*. [Online]. Available: http://www-01.ibm.com/software/commerce/optimization/cplex-optimizer/

[28] Gurobi Optimization, Inc., *Gurobi optimizer*. [Online]. Available: http://www.gurobi.com

[29] MOSEK ApS, *Optimization software*. [Online]. Available: http://www.mosek.com/

[30] S. N. Manias, *Power electronics and motor drive systems*. Cambridge, MA: Academic Press, 2016.

[31] T. Geyer, "A comparison of control and modulation schemes for medium-voltage drives: Emerging predictive control concepts versus PWM-based schemes," *IEEE Trans. Ind. Appl.*, vol. 47, no. 3, pp. 1380–1389, May/Jun. 2011.

[32] J. Holtz, "The representation of ac machine dynamics by complex signal flow graphs," *IEEE Trans. Ind. Electron.*, vol. 42, no. 3, pp. 263–271, Jun. 1995.

Petros Karamanakos (S'10–M'14) received the Diploma and the Ph.D. degrees in electrical and computer engineering from the National Technical University of Athens (NTUA), Athens, Greece, in 2007, and 2013, respectively.

From 2010 to 2011 he was with the ABB Corporate Research Center, Baden-Dättwil, Switzerland, where he worked on model predictive control strategies for medium-voltage drives. From 2013 to 2016 he was a PostDoc Research Associate in the Chair of Electrical Drive Systems and Power Electronics, Technische Universität München, Munich, Germany. He is currently an Assistant Professor in the Faculty of Computing and Electrical Engineering, Tampere University of Technology, Tampere, Finland. His main research interests lie at the intersection of optimal control, mathematical programming and power electronics, including model predictive control for power electronic converters and ac drives.

Dr. Karamanakos received the 2014 Third Best Paper Award of the IEEE Transactions on Industry Applications and the First Prize Paper Award of the Industrial Drives Committee at the 2013 IEEE Energy Conversion Congress and Exposition.

Tobias Geyer (M'08–SM'10) received the Dipl.-Ing. and Ph.D. degrees in electrical engineering from ETH Zurich, Zurich, Switzerland, in 2000 and 2005, respectively. From 2006 to 2008, he was with GE's Global Research Centre, Munich, Germany. Subsequently, he spent three years at the University of Auckland, Auckland, New Zealand. In 2012, he joined ABB's Corporate Research Centre, Baden-Dättwil, Switzerland, where he is currently a Senior Principal Scientist for power conversion control. In 2017, he received a Habilitation degree in power electronics from ETH Zurich, Zurich, Switzerland, and was appointed as an extraordinary professor at Stellenbosch University, South Africa.

His research interests include model predictive control, medium-voltage drives and utility-scale power converters. He is the author of more than 100 peer-reviewed publications, 30 patent applications, and the book "Model predictive control of high power converters and industrial drives", which was published by Wiley in 2016. He teaches a regular course on model predictive control at ETH Zurich.

Tobias was a recipient of the 2014 Third Best Paper Award of the Transactions on Industry Applications. He also received two Prize Paper Awards at conferences. He serves as an Associate Editor for the Transactions on Power Electronics.

Ralph Kennel (M'89–SM'96) received the Diploma and Dr.-Ing. (Ph.D.) degrees from the University of Kaiserslautern, Kaiserslautern, Germany, in 1979 and 1984, respectively.

From 1983 to 1999 he worked on several positions with Robert BOSCH GmbH, Germany. Until 1997, he was responsible for the development of servo drives. He was one of the main supporters of VECON and SERCOS interface, two multicompany development projects for a microcontroller and a digital interface especially dedicated to servo drives. Furthermore, he actively took part in the definition and release of new standards with respect to CE marking for servo drives. Between 1997 and 1999, he was responsible for "Advanced and Product Development of Fractional Horsepower Motors" in automotive applications. His main activity was preparing the introduction of brushless drive concepts to the automotive market. From 1994 to 1999, he was appointed Visiting Professor at the Newcastle University, Newcastle-upon-Tyne, U.K. From 1999 to 2008, he was Professor for Electrical Machines and Drives at Wuppertal University, Wuppertal, Germany. Since 2008 he is Professor for Electrical Drive Systems and Power Electronics at Technische Universtät München, Munich, Germany. His main interests today are sensorless control of ac drives, predictive control of power electronics and hardware-in-the-loop systems.

Dr. Kennel is a Senior Member of IEEE, a Fellow of IEE and a Chartered Engineer in the U.K. Within IEEE, he is Treasurer of the Germany Section as well as ECCE Global Partnership Chair of the Power Electronics Society (PELS). Dr. Kennel has received in 2013 the Harry Owen Distinguished Service Award from IEEE-PELS as well as the EPE Association Distinguished Service Award in 2015. Dr. Kennel was appointed "Extraordinary Professor" by the University of Stellenbosch (South Africa) from 2016 to 2019 and as "Visiting Professor" at the Haixi Institute by the Chinese Academy of Sciences from 2016 to 2021. There he was appointed as "Jiaxi Lu Overseas Guest Professor" in 2017.